Nonlinear profile order for three-dimensional hybrid radial acquisition applied to self-gated free-breathing cardiac cine MRI*

Yanchun Zhu(朱艳春)[1,2], Pascal Spincemaille[2], Jing Liu(刘静)[2], Shuo Li(李硕)[1], Thanh D Nguyen[2], Martin R Prince[2], Yaoqin Xie(谢耀钦)[1,†], and Yi Wang(王乙)[2,‡]

[1] *Institute of Biomedical and Health Engineering, Shenzhen Institute of Advanced Technology, Chinese Academy of Sciences, Shenzhen* 518055, *China*
[2] *Department of Radiology, Weill Cornell Medical College, New York* 10021, *United States*

(Received 23 July 2016; revised manuscript received 23 September 2016; published online 22 December 2016)

This paper presents a nonlinear profile order scheme for three-dimensional (3D) hybrid radial acquisition applied to self-gated, free-breathing cardiac cine magnetic resonance imaging (MRI). In self-gated, free-breathing cardiac cine MRI, respiratory and cardiac motions are unpredictable during acquisition, especially for retrospective reconstruction. Therefore, the non-uniformity of the *k*-space distribution is an issue of great concern during retrospective self-gated reconstruction. A nonlinear profile order with varying azimuthal increments was provided and compared with the existing golden ratio-based profile order. Optimal parameter values for the nonlinear formula were chosen based on simulations. The two profile orders were compared in terms of the *k*-space distribution and phantom and human image results. An approximately uniform distribution was obtained based on the nonlinear profile order for persons with various heart rates and breathing patterns. The nonlinear profile order provides more stable profile distributions and fewer streaking artifacts in phantom images. In a comparison of human cardiac cine images, the nonlinear profile order provided results comparable to those provided by the golden ratio-based profile order, and the images were suitable for diagnosis. In conclusion, the nonlinear profile order scheme was demonstrated to be insensitive to various motion patterns and more useful for retrospective reconstruction.

Keywords: nonlinear profile order, hybrid radial, self-gating, cardiac cine MRI

PACS: 87.61.–c, 87.57.–s **DOI:** 10.1088/1674-1056/26/1/018701

1. Introduction

Two-dimensional (2D) cardiac cine MRI using multiple slices to cover the heart volume is widely employed in clinical practice.[1,2] During 2D cine scanning, multiple breath holds and electrocardiographic (ECG) gating are needed. Varying breath-holding positions causes slice misregistration error (gaps or overlaps between successive slices).[3] In addition, some patients have breath-holding incapability,[4] which will cause motion artefacts. Using ECG gating to synchronise heart motion prolongs patient preparation time and may be infeasible due to magnetohydrodynamic interference.[5,6] In recent years, free breathing, three-dimensional (3D), self-gated techniques without breath holding and ECG gating have been developed and widely studied.[7–17]

Self-gating techniques derive motion signals from internal organs without using peripheral equipment to synchronise respiratory and cardiac motion. There are two primary methods used to obtain respiratory and cardiac self-gating motion signals in cine MRI. First, *k*-space center data, which can reflect changes in image volumes, have been collected to derive respiratory and cardiac motion signals.[9,12–14] Self-gating signals can also be calculated from the image data themselves, but these signals require image reconstruction and registration calculation throughout the cardiac circle.[8,15–17] However, most self-gating methods require breath holds or ECG to avoid the complexity of separating respiratory and cardiac motions.[18,19] A hybrid radial sampling method that uses appropriate band-pass filters to separate respiratory and cardiac motions has been used in both respiratory and cardiac self-gated 3D cine MRI.[7,20] Motions are detected using the centerlines in the slice encoding direction (a process referred to as Cartesian acquisition), and radial sampling of each slice encoding is performed to ensure that *k*-space centerlines are acquired repeatedly. This technique does not require any extra data to obtain self-gating signals. However, the uniformity and stability of the *k*-space distribution is a great concern in retrospective cine MRI.

In this study, a nonlinear angle increment profile order for free-breathing respiratory and cardiac self-gated cardiac cine MRI was put forward. Optimal parameter values for the nonlinear formula were chosen based on simulation results. The proposed profile order was compared with the existing golden

*Project supported by the National Natural Science Foundation of China (Grant Nos. 81501463, 61671026, 81571669, and 81671853), the Natural Science Foundation of Guangdong Province, China (Grant No. 2014A030310360), Guangdong Innovative Research Team Program of China (Grant No. 2011S013), the Basic Research Project of Shenzhen City, China (Grant Nos. JCYJ20140417113430639 and JCYJ20160429172357751), the High-level Oversea Talent Program of Shenzhen City, China (Grant No. KQJSCX20160301144248), and Beijing Center for Mathematics and Information Interdisciplinary Sciences of China.

†Corresponding author. E-mail: yq.xie@siat.ac.cn
‡Corresponding author. E-mail: yiwang@med.cornell.edu

© 2017 Chinese Physical Society and IOP Publishing Ltd

ratio-based profile order in terms of the k-space distribution and phantom and human image results.

2. Materials and methods

2.1. Self-gated pulse sequence

Three-dimensional hybrid radial sampling was used to obtain self-gating signals and acquire k-space data simultaneously. As shown in Fig. 1(a), a 3D steady-state free precession (SSFP) pulse sequence was implemented with a hybrid radial k-space trajectory (Cartesian sampling along the slice encoding direction, k_z, and radial sampling in the k_x–k_y plane). All slices encoded with a specific angle (denoted as the profile) were acquired sequentially before switching to the next angle (Fig. 1(b)). Each profile included n_z slice encodings, limiting the temporal resolution to $n_z TR$. The total number of profiles acquired and used in retrospective reconstruction was predetermined. Therefore, the profile order was determined before the scan.

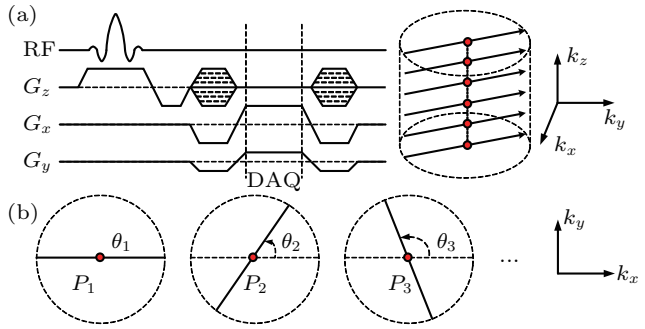


Fig. 1. (color online) SSFP pulse sequence collects the profile with multiple slice encoding lines at a specific angle (a) and changed the profile angle after finishing the last profile (b).

2.2. Nonlinear profile order

The purpose of determining the optimal profile order was to obtain an approximately uniform k-space distribution for each cardiac phase. In the aforementioned hybrid radial scheme, the profile angle is related to the profile number by

$$\theta = \alpha\pi P^{\beta}. \tag{1}$$

In Eq. (1), θ is the profile angle of profile P, and α and β are variables. When $\beta = 1$, the profile angle increases linearly. The golden ratio-based profile order is obtained when $\alpha = 0.618$. However, only continuous profiles alternated by the golden ratio can generate an approximately uniform k-space distribution.[21]

In cine MRI, images are reconstructed from multiple cardiac cycles (see Fig. 2). Each cardiac cycle contains multiple profiles whose number is equal to the number of reconstructed cardiac phases. Suppose that the number of cardiac phases conforms to a normal distribution, $C \sim N(\overline{C}, \sigma)$. The profile in the j-th cardiac cycle, P_j, can be expressed as $P_j = j\overline{C}$. The profile angle θ in Eq. (1) can then be replaced by

$$\theta_j = \alpha\pi\left(j\overline{C}\right)^{\beta} = \alpha\overline{C}^{\beta}\pi j^{\beta}. \tag{2}$$

Technically, because of the existence of $\overline{C}$, the golden ratio condition is not satisfied. In the self-gated free breathing method, data acquired within a given window in a respiratory histogram are used for image reconstruction. For respiratory gating, a rectangular waveform function $\Pi\left(\frac{P}{\overline{R}}\right)$, where $\overline{R}$ is the mean period of respiratory motion, is used to filter data into the respiratory gating window. After respiratory and cardiac gating, the profile angle θ_j satisfies

$$\theta_j = \alpha\pi P_j^{\beta}\Pi\left(\frac{P_j}{\overline{R}}\right) = \alpha\pi\left(j\overline{C}\right)^{\beta}\Pi\left(\frac{j\overline{C}}{\overline{R}}\right). \tag{3}$$

For view sharing,[22] neighbouring profiles are always shared in the reconstruction. Based on Eq. (1), $\frac{\pi}{3}P$ is appended to Eq. (4) to make neighbouring profiles rotate by $\frac{\pi}{3}$.

$$\theta = \alpha\pi P^{\beta} + \frac{\pi}{3}P. \tag{4}$$

Therefore, for view sharing, profiles after respiratory and cardiac gating satisfy

$$\theta_j = \alpha\pi\left(j\overline{C}\right)^{\beta}\Pi\left(\frac{j\overline{C}}{\overline{R}}\right) + \frac{\pi}{3}\cdot j\overline{C}. \tag{5}$$

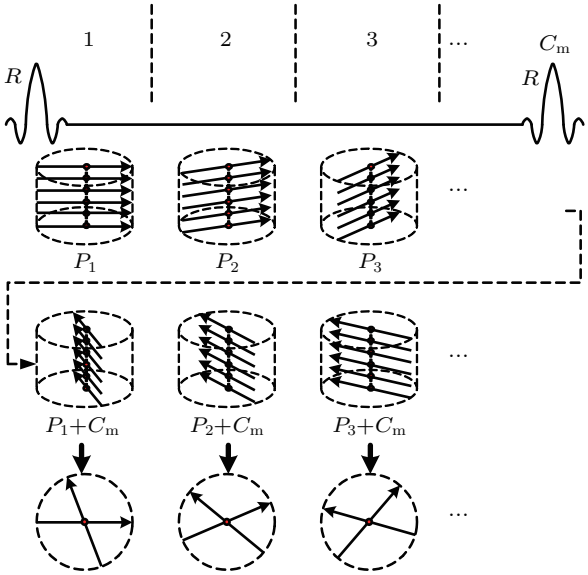


Fig. 2. Cine images reconstructed from multiple cardiac cycles.

2.3. Optimisation of variable parameters

Compared with a uniform distribution, the sample density along the azimuthal direction is not homogeneous, which may affect the image signal-to-noise ratio (SNR). The ratio of the non-uniform $\mathrm{SNR}_{\mathrm{nonun}}$ to the uniform $\mathrm{SNR}_{\mathrm{un}}$ is equal to the sampling efficiency (SE), which depends on the homogeneity of the sample distribution achieved by each acquisition scheme.[21] This ratio is given by

$$\mathrm{SE} = \frac{\mathrm{SNR}_{\mathrm{nonun}}}{\mathrm{SNR}_{\mathrm{un}}} = \sqrt{\frac{\pi^2/M}{\sum_{j=1}^{M}\Delta\theta_i^2}}. \tag{6}$$

Here, $\Delta\theta_i$ is the mean azimuthal distance from the i-th profile to its adjacent profiles, and M is the total number of profiles in the image reconstruction.

The optimal values of the variables α and β were determined by simulation to minimize SE for a cardiac frequency range of 0.6–3 Hz, and a breath frequency range of 0.1–0.5 Hz. Ranges of α (0–2) and β (0–1) values in increments of 0.01 were evaluated. The coefficient of variation (CV) was used to evaluate the SE for different cardiac and breath frequencies.

2.4. Evaluation of clinical scans

Ten normal volunteers (eight male and two female, mean age of 32 years $\pm$ standard deviation of 7 years), without any history or symptoms of cardiac disease, were studied. Cardiac cine imaging was performed in the supine position using a 1.5-T GE HDx scanner (maximum gradient amplitude 33.0 mT/m, slew rate 120 T/m/s, Excite 14 M5 software version; GE Healthcare, Waukesha, WI, USA). All subjects provided written informed consent, and the study was approved by the local institutional ethics review board at Weill Cornell Medical College. An eight-channel cardiac phased-array coil was used for signal reception.

Two separate scans were executed in random order using the same imaging parameters. The typical imaging parameters were as follows: TR/TE = 4.4/1.3 ms, flip angle is 40°, readout bandwidth is $\pm$125 kHz, field of view is 31 cm, reconstructed image matrix is 256×256, slice thickness is 10 mm, and number of slice encodings is 12–14. The temporal resolution ranged from 52.8 to 61.6 ms, depending on the number of slices. The total number of profiles was 5000, and the total free-breathing 3D acquisition time was approximately 5 min.

It was impossible to ensure that the volunteers maintained the same breathing and heart rate patterns during the two continuous scans. To compare the two profile orders using the same standards, the SEs calculated using Eq. (6) were also compared for the same self-gating motion signals obtained from the above acquisitions.

2.5. Evaluation of phantom simulation

The optimised nonlinear profile order was compared with the golden ratio-based profile order. A phantom was sampled using these two profile orders. The original k-space data for the phantom were selected based on self-gating signals from the ten volunteers. Twenty phantom images obtained using these two methods were compared in terms of the SNR.

2.6. Statistical analysis of image quality

Image quality metrics, including the blood SNR, myocardium-blood contrast, contrast-to-noise ratio (CNR), and image sharpness,[8] were calculated from a mid-ventricular slice for each volunteer. The two methods were compared using a nonparametric Wilcoxon signed-rank test. All of the tests were two-sided, and $P < 0.05$ was considered to indicate a significant difference. The statistical analyses were performed using statistical software (SPSS version 19; SPSS Inc., Chicago, IL, USA). Values are reported herein as means $\pm$ standard deviations.

3. Results

3.1. Optimisation of variable parameters

Figure 3 shows the SE CV values corresponding to various α and β values. Low CV values are inversed in brightness in Fig. 3(a). Low SE CV values for various combinations of cardiac and respiratory frequencies improve the adaptability of the sampling method. The lowest CV values for each α are shown as red dots in Fig. 3(a). The α and β value pairs had similar CV values (5% difference), as shown in Fig. 3(b). The combination of $\alpha = 0.32$ and $\beta = 0.46$ was identified as optimal, i.e., as yielding the lowest CV of the SE.

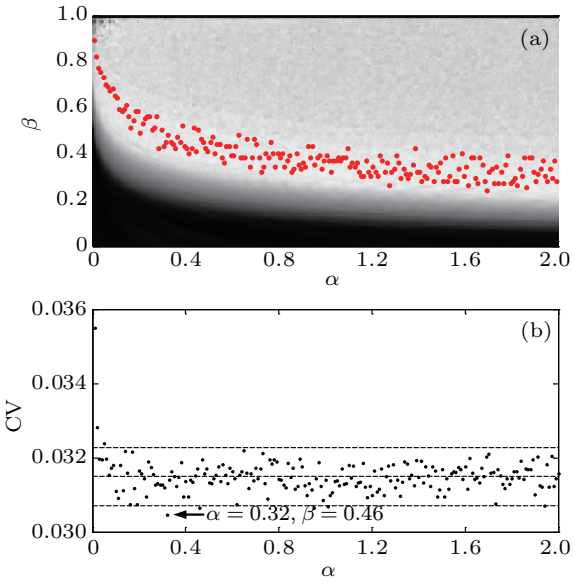


Fig. 3. (color online) (a) CV of SE corresponding to different α and β values, and smaller CV values were inversed to bright for optimal viewing. The minimal CV values according to each α are indicated as red dots. CV values at red dots are plotted in panel (b).

3.2. Clinical scan

Image reconstruction was performed for the ten subjects, for one of whom the golden ratio method had failed. Figure 4 shows images of mid-ventricular slices obtained during end-diastolic and end-systolic cardiac phases from the other volunteers. The two methods were compared to each other. A few streaking artefacts appeared in both sampling methods because of undersampling (the undersampling ratio was 2:3) and motion. Table 1 summarises the metrics of image quality for the mid-ventricular images shown in Fig. 4. Comparable image quality metrics were obtained for blood SNR, myocardium-blood CNR, myocardium contrast, and image sharpness. The differences were not statistically significant ($P > 0.05$).

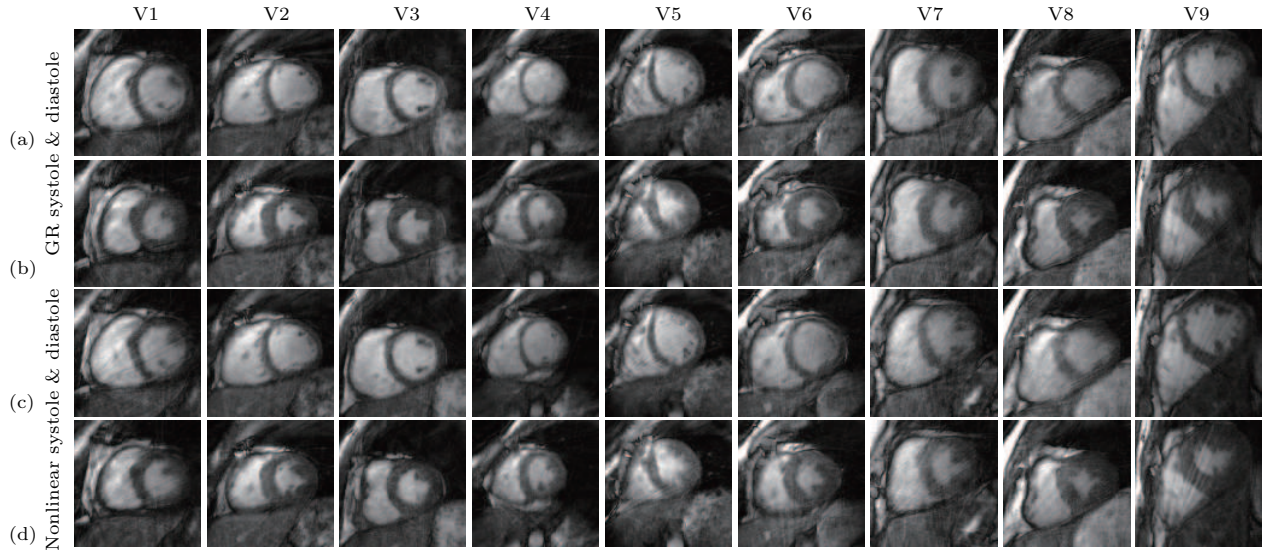


Fig. 4. (a), (b) Images of mid-ventricular slices obtained with golden ratio-based profile order and (c), (d) nonlinear profile order in nine healthy volunteers.

Table 1. Metrics of image quality of the two methods ($N = 9$).

	SNR_{Blood}	$CNR_{Blood-Myocardium}$	$Contrast_{Blood-Myocardium}$	Image sharpness/mm^{-1}
Golden ratio diastole	53.5±25.3	22.0±14.8	24.7±6.9	0.21±0.04
Nonlinear diastole	54.4±28.5	22.2±17.0	24.4±9.9	0.24±0.03
P-value	0.767	0.678	0.767	0.110
Golden ratio systole	54.4±18.6	22.1±10.7	24.7±6.8	0.22±0.05
Nonlinear systole	51.9±21.0	22.2±13.7	26.2±11.4	0.26±0.07
P-value	0.173	0.678	0.515	0.086

Figure 5 shows a comparison of the SE for the golden ratio and nonlinear profile orders for the real self-gating signals obtained. For the same respiratory and cardiac self-gating signals, profiles from the nonlinear method had higher mean SE values (nonlinear: 0.831 ± 0.02; golden ratio: 0.80 ± 0.11), which means that the nonlinear profile order provided a more uniform distribution for the same number of profiles. As indicated by the arrows in Fig. 5, the golden ratio-based profile orders generated worse *k*-space distributions (SE = 0.35) than the nonlinear profile orders (SE = 0.86). The SE difference between the two methods was not statistically significant ($p = 0.60$), according to the results of a two-sided Wilcoxon signed-rank test.

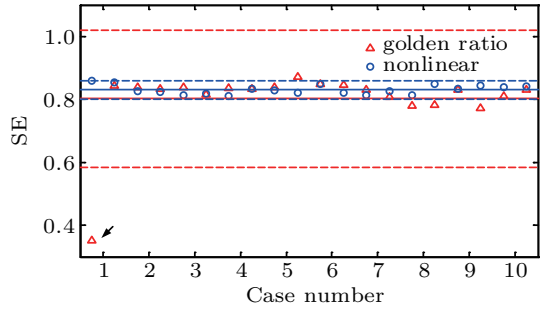


Fig. 5. (color online) Comparison of SE between golden ratio and nonlinear profile orders based on the same self-gating signals.

3.3. Phantom simulation

The SNRs determined for phantom images of golden ratio-based and nonlinear profile orders were 164.45 ± 22.81 and 176.55 ± 23.83, respectively. Figure 6 shows reconstructed phantom images and profile distributions based on the self-gating signals for a subject for whom the golden

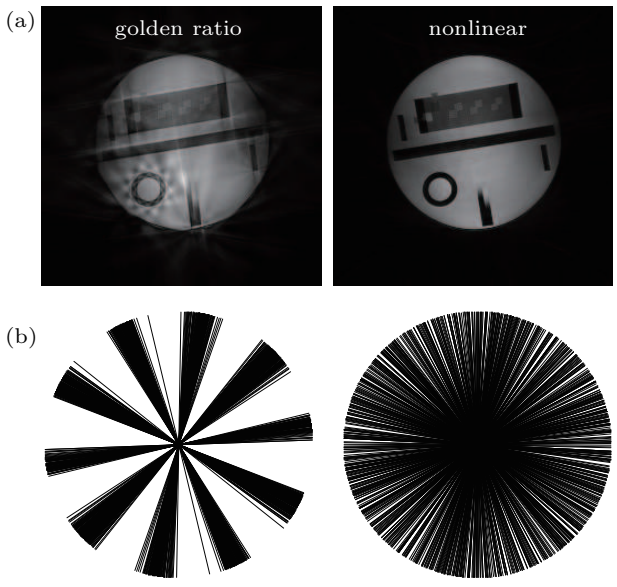


Fig. 6. (a) Reconstructed phantom images and (b) profile distribution based on the same self-gating signals from failed subject, which is indicated by the arrow in Fig. 5.

ratio-based profile order failed (as indicated by an arrow in Fig. 5). Nearly 353 profiles were used in the reconstruction, including shared neighbouring profiles. Obvious streak artefacts appeared in the golden ratio-based profile order as a result of the non-uniform distribution of the profiles. More uniform distributions were generated based on the nonlinear profile order (SE for golden ratio is 0.35; SE for nonlinear is 0.86).

4. Discussion and conclusions

It has been demonstrated that a self-gated approach permits accurate and reliable assessment of right-ventricle (RV) and left-ventricle (LV) cardiac dimensions without using ECG triggers and respiratory monitors.[7,20] In free-breathing, self-gated cardiac cine MRI, respiratory and cardiac motions are unpredictable before acquisition. Therefore, non-uniform k-space distribution is a major problem in retrospective self-gated reconstruction. In this study, a nonlinear profile order with varying azimuthal increments was proposed as an alternative to the golden ratio-based profile order.

Approximately uniform distributions were obtained for individuals with different heart rates and breathing patterns in both simulations and clinical acquisition of self-gating signals. The acquisition scheme for the golden ratio-based profile failed to provide the nearly uniform profile distribution in 3D hybrid radial SSFP acquisition in the study subjects. In the 3D hybrid radial acquisition scheme, interbeat (R–R) intervals limited the profile number to a range of 15–22, which was equal to the number of cardiac phases $\overline{C}$. Based on Eq. (2) ($\theta_j = \alpha \cdot \overline{C}^{\beta} \pi j^{\beta}$), the profile distribution is related to $\overline{C}$. The alternative angle of the profiles in the same cardiac phase is $\alpha\overline{C}\pi$. Therefore, the profile distribution was different from person to person. As Fig. 5 shows, the golden ratio-based profile order failed to provide a uniform distribution for one subject. This problem cannot be solved by using a sliding window, as shown in Fig. 6(b). The specified $\overline{C}$ values and proportions of failure were out of range in this study. The proposed nonlinear profile acquisition scheme provided a nearly uniform profile distribution for all of the study subjects for cardiac motion frequencies in the range of 0.6–3 Hz and respiratory frequencies in the range of 0.1–0.5 Hz.[9] This indicates some distinct advantages of the proposed nonlinear profile acquisition scheme in comparison to conventional radial and golden ratio-based profile acquisition schemes.

The primary advantage of the nonlinear profile order is its insensitivity to the heart rate and breathing rate. Because the minimal CV of the SE (Eq. (6)) was pursued in the simulation, the nonlinear profile order obtained can be applied to persons with different heart and breathing rates. Moreover, $\pi P/3$ was added to Eq. (4) for the purpose of view sharing, which introduces at least $\pi/3$ alternate profile angles between neighboring profiles. Considering eddy currents, the $\pi/3$ alternate angles could be removed when view sharing is not considered. Smaller eddy currents will be induced than with golden alternate angles, and the eddy currents can deviate from the center of the k-space. This could lead to jitter and drift in the cardiac and respiratory signals detected.[12] Therefore, another potential advantage of the nonlinear profile order is reduced production of eddy currents. This will be examined further in future research.

The proposed profile order was constructed and simulated on the basis of a specified hybrid radial profile order and was specified for use in retrospective cine MRI. For these circumstances, the golden ratio-based profile order was found to be unstable for different persons. This finding is not in conflict with other applications based on golden means. Fewer total profile numbers could be used to reduce the total scan time by using compressed sensing (CS) reconstruction. However, the optimal α and β values will differ from other total profile numbers. The simulation should therefore be repeated for other total profile numbers. Although this requirement is a clear limitation of the nonlinear profile order method, additional research will be conducted to establish the optimal α and β values for the usual profile numbers.

In conclusion, this paper presents a nonlinear profile order for 3D hybrid radial acquisition for use in cardiac and respiratory self-gated cine MRI. A more stable profile distribution is obtained during retrospective reconstruction using the proposed profile order than using a golden ratio-based profile order. Three-dimensional short-axis-view cine imaging with the proposed profile order achieves image quality comparable to that achievable with the existing golden ratio-based profile order.

Acknowledgments

The authors would like to thank all colleagues from the Department of Radiology, Weill Medical College of Cornell University, NY, for providing help in data collection. The founders had no role in study design, data collection and analysis, decision to publish, or preparation of the manuscript.

References

[1] Beygui F, Furber A, Delepine S, Helft G, Metzger J P, Geslin P and Le Jeune J J 2004 *The International Journal of Cardiovascular Imaging* **20** 509
[2] Omoumi P, Metais J, Bertrand P and Alison D 2010 *Journal de radiologie* **91** 769
[3] Swingen C, Seethamraju R T and Jerosch-Herold M 2003 *The International Journal of Cardiovascular Imaging* **19** 325
[4] Jahnke C, Paetsch I, Achenbach S, Schnackenburg B, Gebker R, Fleck E and Nagel E 2006 *Radiology* **239** 71
[5] Damji A, Snyder R, Ellinger D, Witkowski F and Allen P 1988 *Magnetic Resonance Imaging* **6** 637
[6] Shetty A 1988 *Magnetic Resonance in Medicine* **8** 84
[7] Liu J, Spincemaille P, Codella N, Nguyen T, Prince M and Wang Y 2010 *Magnetic Resonance in Medicine* **63** 1230
[8] Larson A C, Kellman P, Arai A, Hirsch G A, McVeigh E, Li D and Simonetti O P 2005 *Magn Reson Med* **53** 159

[9] Buehrer M, Curcic J, Boesiger P and Kozerke S 2008 *Magnetic Resonance in Medicine* **60** 683

[10] Larson A, White R, Laub G, McVeigh E, Li D, and Simonetti O 2004 *Magnetic Resonance in Medicine* **51** 93

[11] Hiba B, Richard N, Thibault H, and Janier M 2007 *Magn. Reson. Med.* **58** 745

[12] Manka R, Buehrer M, Boesiger P, Fleck E and Kozerke S 2010 *Radiology* **255** 909

[13] Spincemaille P, Nguyen T, Prince M and Wang Y 2008 *Magnetic Resonance in Medicine* **60** 158

[14] Uribe S, Muthurangu V, Boubertakh R, Schaeffter T, Razavi R, Hill D and Hansen M 2007 *Magnetic Resonance in Medicine* **57** 606

[15] Crowe M, Larson A, Zhang Q, Carr J, White R, Li D and Simonetti O 2004 *Magnetic Resonance in Medicine* **52** 782

[16] Leung A O, Paterson I and Thompson R B 2008 *Magnetic Resonance in Medicine* **60** 709

[17] Spraggins T 1990 *Magnetic Resonance Imaging* **8** 675

[18] Liu J, Wieben O, Jung Y, Samsonov A, Reeder S and Block W 2010 *Journal of Magnetic Resonance Imaging* **32** 434

[19] Spincemaille P, Liu J, Nguyen T, Prince M R and Wang Y 2011 *Magnetic Resonance Imaging* **29** 861

[20] Zhu Y, Liu J, Weinsaft J, Spincemaille P, Nguyen T D, Prince M R, Bao S, Xie Y and Wang Y 2015 *BioMed Research International* **2015** 819102

[21] Winkelmann S, Schaeffter T, Koehler T, Eggers H and Doessel O 2007 *IEEE Transactions on Medical Imaging* **26** 68

[22] Liu J, Redmond M, Brodsky E, Alexander A, Lu A, Thornton F, Schulte M, Grist T, Pipe J and Block W 2006 *IEEE Transactions on Medical Imaging* **25** 148